small
www.small-journal.com

Cu^{2+}-Modified Metal–Organic Framework Nanoparticles: A Peroxidase-Mimicking Nanoenzyme

*Wei-Hai Chen, Margarita Vázquez-González, Anna Kozell, Alessandro Cecconello, and Itamar Willner**

The synthesis and characterization of UiO-type metal–organic framework nanoparticles (NMOFs) composed of Zr^{4+} ions bridged by 2,2′-bipyridine-5,5′-dicarboxylic acid ligands and the postmodification of the NMOFs with Cu^{2+} ions are described. The resulting Cu^{2+}-modified NMOFs, Cu^{2+}-NMOFs, exhibit peroxidase-like catalytic activities reflected by the catalyzed oxidation of Amplex-Red to the fluorescent Resorufin by H_2O_2, the catalyzed oxidation of dopamine to aminochrome by H_2O_2, and the catalyzed generation of chemiluminescence in the presence of luminol/H_2O_2. Also, the Cu^{2+}-NMOFs mimic NADH peroxidase functions and catalyze the oxidation of dihydronicotinamide adenine dinucleotide, NADH, to nicotinamide adenine dinucleotide, NAD^+, in the presence of H_2O_2. The Cu^{2+}-NMOFs-catalyzed generation of chemiluminescence in the presence of luminol/H_2O_2 is used to develop a glucose sensor by monitoring the H_2O_2 formed by the aerobic oxidation of glucose to gluconic acid in the presence of glucose oxidase. Furthermore, loading the Cu^{2+}-NMOFs with fluorescein and activating the catalyzed generation of chemiluminescence in the presence of luminol/H_2O_2 yield an efficient chemiluminescence resonance energy transfer (CRET) process to the fluorescein reflected by the activation of the fluorescence of the dye (λ = 520 nm, CRET efficiency 35%).

Metal–organic frameworks (MOFs) represent a broad class of porous materials composed of metal ions cross-linked by organic ligands.[1] Besides the interesting structural features of MOFs,[2] many different applications of MOFs were reported[3] including their use as drug carriers,[4] catalysts,[5] sensors,[6] gas storage,[7] separation,[8] optical devices,[9] photocatalysts,[10] and as micromotors.[11] The use of the highly porous MOFs as structural scaffolds for the development of catalysts is particularly interesting.[12] Different methods to synthesize MOF-based catalysts were developed and these included the incorporation of catalytic complexes into the pores of the MOFs,[13] the incorporation of metal complexes as functional ligands of the MOF frameworks,[14] and the construction of MOFs that include ligands for the postsynthetic anchoring of metal ions and the formation of catalytic sites.[15] Many different chemical transformations were driven by catalytic MOFs, such as Friedel–Crafts alkylation reaction,[16] hydrogenation,[17] and oxidation.[18]

Recent research efforts are directed to the use of nanomaterials or inorganic nanoparticles as peroxidase-mimicking catalysts. Hemin/G-quadruplex structures,[19] metal nanoclusters, or nanoparticles, such as Au,[20] Cu,[21] Pt,[22] or metal oxide nanoparticles,[23] e.g., Fe_2O_3 or TiO_2 and carbon-based nanomaterials such as Cu^{2+}-modified carbon dots,[24] carbon nitride,[24] and graphene oxide[25] reveal peroxidase-like functions. Also, hemin embedded in MOFs,[13] and metal-ion-functionalized MOFs revealed, in analogy to horseradish peroxidase (HRP), the generation of chemiluminescence[26] by the catalyzed oxidation of luminol by H_2O_2.

In the present study, we report on the synthesis of UiO-type MOF nanoparticles[27] (NMOFs) composed of Zr^{4+} ions bridged by 2,2′-bipyridine-5,5′-dicarboxylic acid ligands, (**1**), followed by the postmodification of the bipyridine ligands with Cu^{2+} ions. The Cu^{2+}-modified NMOFs (Cu^{2+}-NMOFs) reveal peroxidase-mimicking activities. In contrast to previous studies[28] reporting peroxidase-mimicking functions of MOFs containing metal ions such as Cu^{2+} and Fe^{3+}, which are part of the frameworks, the present catalytic NMOFs include a metal-ion ligand (bipyridine) as a part of the framework, and the complexation of metal ions, e.g., Cu^{2+} to the ligand, yield the catalytic peroxidase-mimicking NMOFs. The peroxidase-mimicking functions of the Cu^{2+}-NMOFs are reflected by the catalyzed oxidation of Amplex-Red by H_2O_2 to form Resorufin, the catalyzed H_2O_2-driven oxidation of dopamine to aminochrome, and the catalyzed generation of chemiluminescence in the presence of luminol/H_2O_2. The Cu^{2+}-NMOFs-catalyzed generation of chemiluminescence in the presence of luminol/H_2O_2 was further used to develop a chemiluminescence glucose sensor based on the aerobic oxidation of glucose in the presence of glucose oxidase. Also, the Cu^{2+}-NMOFs catalyze the oxidation of dihydronicotinamide adenine dinucleotide, NADH, by H_2O_2 to form nicotinamide adenine dinucleotide, NAD^+, as a NADH peroxidase-mimicking "nanoenzyme" is described. Finally, by the incorporation of the fluorescein dye into the pores of the NMOFs the chemiluminescence generated by the NMOFs induces a highly efficient chemiluminescence resonance energy

Dr. W.-H. Chen, Dr. M. Vázquez-González, A. Kozell, Dr. A. Cecconello, Prof. I. Willner
Institute of Chemistry
Center for Nanoscience and Nanotechnology
The Hebrew University of Jerusalem
Jerusalem 91904, Israel
E-mail: willnea@vms.huji.ac.il

The ORCID identification number(s) for the author(s) of this article can be found under https://doi.org/10.1002/smll.201703149.

DOI: 10.1002/smll.201703149

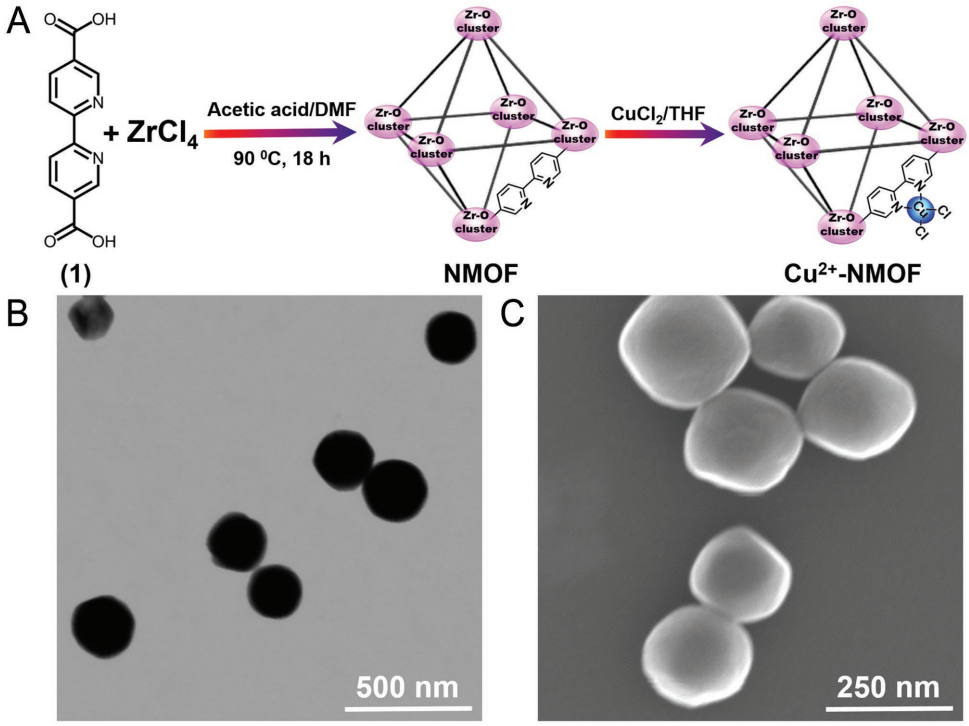

Figure 1. A) Synthesis of the Cu^{2+}-functionalized Zr^{4+}-5,5′-bipyridine carboxylate-bridged metal–organic framework nanoparticles (NMOFs). B) TEM image of the NMOFs. C) SEM image of the NMOFs.

transfer (CRET) process resulting in the fluorescence of fluorescein, $\lambda = 520$ nm. The unprecedented efficient CRET process is attributed to the porous structure of the NMOFs that allows the concentration of the energy acceptor dye in close proximity to the chemiluminescence generating sites.

The NMOFs revealed a bipyramidal structure, ≈200 nm (**Figure 1**). The powder X-ray diffraction spectra of the NMOFs before and after modification with Cu^{2+} ions are identical (Figure S1, Supporting Information) implying that the structure of the NMOFs remains intact after modification with the Cu^{2+} ions. The surface area and pore sizes of the Cu^{2+}-modified NMOFs correspond to 246 m^2 g^{-1} and 1.65 nm, respectively (surface area and pore size of the NMOFs prior to the modification with Cu^{2+} 738 m^2 g^{-1} and 1.99 nm, respectively). The resulting Cu^{2+}-NMOFs were also characterized by X-ray photoelectron spectroscopy (see Figure S2, Supporting Information, and the accompanying discussion) and Fourier transform infrared spectra (see Figure S3, Supporting Information). The content of Cu^{2+} ions in the Cu^{2+}-NMOFs was determined by inductively coupled plasma atomic emission spectroscopy analysis and it corresponds to 5.5 wt% in the Cu^{2+}-NMOFs.

The Cu^{2+}-NMOFs mimic the function of HRP and catalyze the oxidation of Amplex-Red to the fluorescent Resorufin by H_2O_2 (**Figure 2**A). The fluorescence spectra of Resorufin

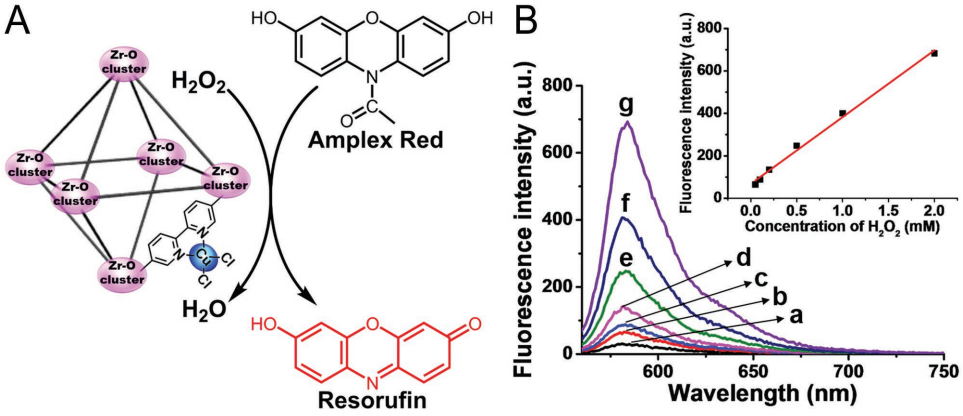

Figure 2. A) Schematic Cu^{2+}-NMOFs-catalyzed oxidation of Amplex-Red to the fluorescent Resorufin product by H_2O_2. B) Fluorescence spectra of the Resorufin product generated in the catalyzed oxidation of Amplex-Red, 0.2×10^{-3} M, by Cu^{2+}-NMOFs, 20 μg mL^{-1}, using different concentrations of H_2O_2: (a) 0 M, (b) 0.05×10^{-3} M, (c) 0.1×10^{-3} M, (d) 0.2×10^{-3} M, (e) 0.5×10^{-3} M, (f) 1×10^{-3} M, (g) 2×10^{-3} M. Inset: derived calibration curve corresponding to the fluorescence intensities of Resorufin generated by variable concentrations of H_2O_2.

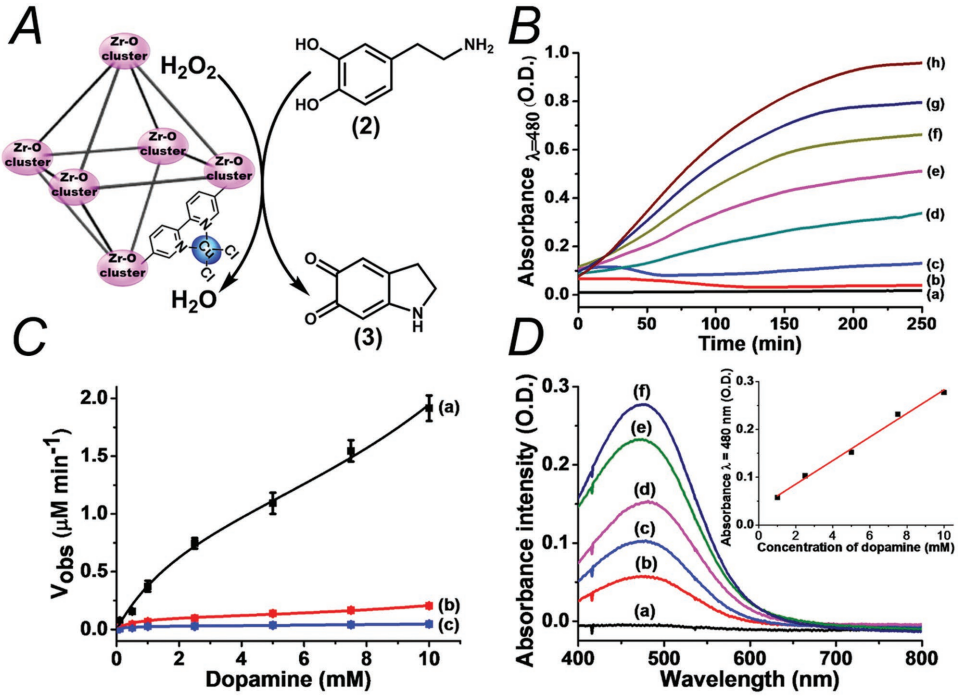

Figure 3. A) Schematic Cu^{2+}-NMOFs-catalyzed oxidation of dopamine by H_2O_2 to form aminochrome. B) Time-dependent absorbance changes upon the Cu^{2+}-NMOFs-catalyzed oxidation of different concentrations of dopamine: (a) 0 M, (b) 0.1×10^{-3} M, (c) 0.5×10^{-3} M, (d) 1×10^{-3} M, (e) 2.5×10^{-3} M, (f) 5×10^{-3} M, (g) 7.5×10^{-3} M, (h) 10×10^{-3} M. In all experiments H_2O_2 10×10^{-3} M and Cu^{2+}-NMOFs 20 μg mL^{-1} were used. C) Rates of the oxidation of dopamine to aminochrome as a function of dopamine concentration by the Cu^{2+}-NMOFs, and the respective control systems: (a) Cu^{2+}-NMOFs 20 μg mL^{-1}, (b) Cu^{2+} ions and the bipyridine ligand, each concentration is 17.3×10^{-6} M (at similar molar ratio to those of Cu^{2+}/bipyridine ligand present in the NMOFs). (c) Cu^{2+} ions only, 17.3×10^{-6} M. In all experiments H_2O_2 10×10^{-3} M was used. D) Absorbance spectra of the Cu^{2+}-NMOFs generated aminochrome by the catalyzed oxidation of different concentrations of dopamine for a fixed time interval of 30 min using Cu^{2+}-NMOFs 20 μg mL^{-1}, H_2O_2 10×10^{-3} M: (a) 0×10^{-3} M, (b) 1×10^{-3} M, (c) 2.5×10^{-3} M, (d) 5×10^{-3} M, (e) 7.5×10^{-3} M, (f) 10×10^{-3} M. Inset: derived calibration curve corresponding to the absorbance of the resulting aminochrome as a function of the concentrations of dopamine.

generated upon oxidation of Amplex-Red in the presence of different concentrations of H_2O_2 and Cu^{2+}-NMOFs, 20 μg mL^{-1}, for a fixed time interval of 30 min are depicted in Figure 2B and the derived calibration curve is shown in the inset of Figure 2B.

Similarly to HRP, the Cu^{2+}-NMOFs catalyze the H_2O_2-driven oxidation of dopamine (**2**) to aminochrome (**3**) (**Figure 3**A). The time-dependent absorbance changes upon formation of aminochrome in the presence of different concentrations of dopamine, (**2**), are shown in Figure 3B. As the concentrations of dopamine increase, the formation of aminochrome is enhanced. Control experiments revealed that the H_2O_2-stimulated catalyzed oxidation of dopamine in the presence of only Cu^{2+} ions or in the presence of Cu^{2+} ions and the bipyridine ligand (at similar molar ratio to those of Cu^{2+}/bipyridine ligand present in the NMOFs) lead to very inefficient oxidation of dopamine by H_2O_2 (Figure 3C, curves (a), (b) and (c), respectively). Presumably, the porous structure of the NMOFs or cooperative effects of adjacent Cu^{2+}-bpy complexes associated with the NMOFs lead to the concentration of dopamine at the catalytic sites. Further support that dopamine is concentrated in the porous Cu^{2+}-NMOFs structure was obtained by complementary Brunauer–Emmett–Teller (BET) measurements. While the Cu^{2+}-NMOFs exhibited a surface area of 246 m^2 g^{-1} and average pore sizes of 1.65 nm, the Cu^{2+}-NMOFs treated with dopamine revealed a surface area corresponding to 150 m^2 g^{-1} and average pore sizes of 1.31 nm. The lower surface area and decreased pore size of the Cu^{2+}-NMOFs treated with dopamine are consistent with the occupation of the pores with dopamine. The effective incorporation of dopamine into the NMOFs is further supported by ^{1}H-NMR experiments (Figure S4, Supporting Information). The Cu^{2+}-NMOFs were treated with dopamine, 10×10^{-3} M, and the resulting NMOFs were separated. The ^{1}H-NMR spectrum of the resulting NMOFs is shown in Figure S4 (Supporting Information). By the integration of the protons associated with dopamine and the NMOFs ligands we conclude that the molar ratio of dopamine:NMOFs ligand is 5:1. (For further discussion of the molar ratio of dopamine to NMOFs, see Figure S4, Supporting Information.) The oxidation of dopamine is controlled by the concentration of the Cu^{2+}-NMOFs catalyst, and as the concentration of the NMOFs increases the oxidation of dopamine is faster (Figure S5, Supporting Information). The absorbance spectra of the aminochrome, (**3**), generated upon oxidation of different concentrations of dopamine by H_2O_2, 10×10^{-3} M, in the presence of 20 μg mL^{-1} of the Cu^{2+}-NMOFs for a fixed time interval of 60 min are depicted in Figure 3D, and the derived calibration curve is displayed in the inset of Figure 3D. In a further control experiment, the Cu^{2+}-NMOFs were treated with the reaction solution for a time interval of 5 h and, subsequently, the Cu^{2+}-NMOFs were precipitated and separated. The resulting solution did not show any catalytic activity toward oxidation of

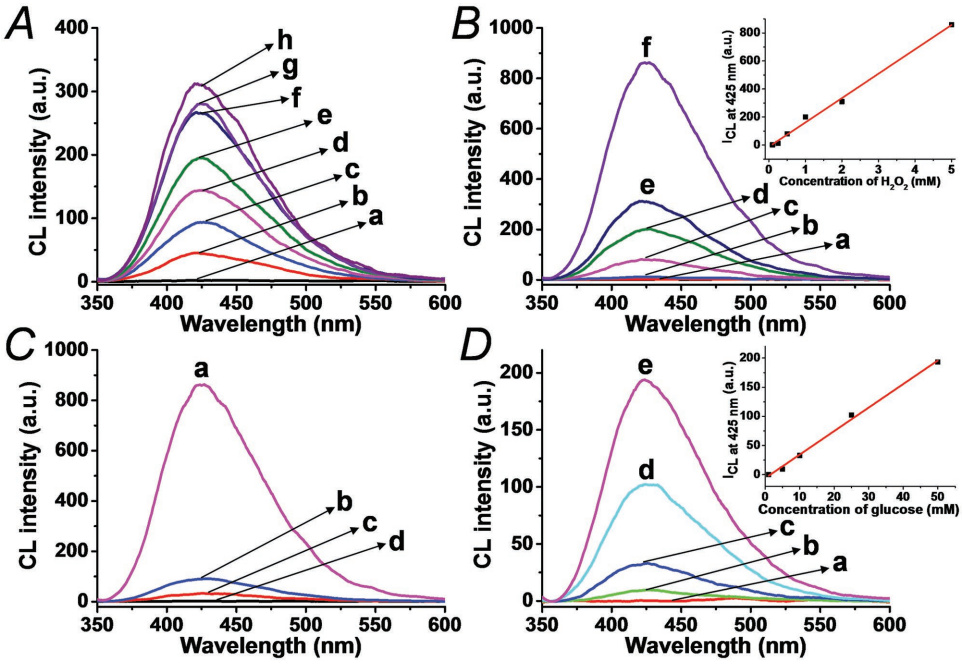

Figure 4. A) Chemiluminescence spectra generated by the Cu^{2+}-NMOFs-catalyzed oxidation of different concentrations of luminol by H_2O_2: (a) 0 M, (b) 0.01×10^{-3} M, (c) 0.025×10^{-3} M, (d) 0.05×10^{-3} M, (e) 0.075×10^{-3} M, (f) 0.1×10^{-3} M, (g) 0.25×10^{-3} M, (h) 0.5×10^{-3} M. In all experiments Cu^{2+}-NMOFs 100 μg mL^{-1} and H_2O_2 2×10^{-3} M were used. B) Chemiluminescence spectra generated by the Cu^{2+}-NMOFs-catalyzed oxidation of luminol, 0.5×10^{-3} M, using different concentrations of H_2O_2: (a) 0.1×10^{-3} M, (b) 0.25×10^{-3} M, (c) 0.5×10^{-3} M, (d) 1×10^{-3} M, (e) 2×10^{-3} M, (f) 5×10^{-3} M. In all experiments Cu^{2+}-NMOFs 100 μg mL^{-1} were used. Inset: derived calibration curve. C) Chemiluminescence spectra generated by the Cu^{2+}-NMOFs in the presence of luminol/H_2O_2 and control systems: (a) Cu^{2+}-NMOFs 100 μg mL^{-1}, (b) Cu^{2+} ions and the bipyridine ligand, each concentration is 86.6×10^{-6} M, (c) Cu^{2+} ions only, 86.6×10^{-6} M, (d) NMOFs without Cu^{2+}. In all experiments luminol 0.5×10^{-3} M and H_2O_2 5×10^{-3} M were used. D) Sensing of glucose via the Cu^{2+}-NMOFs-catalyzed oxidation of luminol generated by the aerobic GOx-catalyzed oxidation of different concentrations of glucose. Chemiluminescence spectra were recorded after a fixed time interval of 30 min at which the GOx-catalyzed oxidation of glucose was allowed to generate H_2O_2. The concentrations of glucose corresponded to: (a) 1×10^{-3} M, (b) 5×10^{-3} M, (c) 10×10^{-3} M, (d) 25×10^{-3} M, (e) 50×10^{-3} M. In all experiments Cu^{2+}-NMOFs 100 μg mL^{-1}, GOx 4 U mL^{-1}, and luminol 0.5×10^{-3} M were used. Inset: derived calibration curve.

dopamine, upon addition of dopamine/H_2O_2, implying that no leakage of Cu^{2+}-ligand complex or degradation of the NMOFs occurred within this time interval. Furthermore, the Cu^{2+}-NMOFs used to catalyze the oxidation of dopamine by H_2O_2 could be separated, and reused for the secondary oxidation of dopamine by H_2O_2 with no noticeable decrease in the catalytic activity of the Cu^{2+}-NMOFs. In fact, such repeated recycling of the Cu^{2+}-NMOFs was performed for five cycles with no loss in the catalytic functions of the nanoparticles.

The Cu^{2+}-NMOFs also catalyze the oxidation of luminol by H_2O_2 resulting in the generation of chemiluminescence (Figure S6, Supporting Information). **Figure 4**A shows the chemiluminescence spectra generated in the presence of different concentrations of luminol (fixed concentrations of H_2O_2, 2×10^{-3} M, and Cu^{2+}-NMOFs, 100 μg mL^{-1}), and Figure 4B depicts the chemiluminescence spectra in the presence of different concentrations of H_2O_2 (fixed concentrations of luminol, 0.5×10^{-3} M, and Cu^{2+}-NMOFs, 100 μg mL^{-1}). As the concentration of H_2O_2 increases, the chemiluminescence spectra are intensified. The resulting calibration curve is presented in Figure 4B (inset). For the dependence of the chemiluminescence spectra on the concentration of the Cu^{2+}-NMOFs see Figure S7 (Supporting Information). Control experiments reveal that the Cu^{2+}-NMOFs are essential to generate the chemiluminescence (Figure 4C). Cu^{2+} ions alone or Cu^{2+} ions and the bipyridine ligand at the same molar concentrations existing in the NMOFs yield only trace intensities of chemiluminescence. Presumably, the concentration of the luminol in the porous NMOFs, in close spatial proximity to the Cu^{2+}-bipyridine MOF units, leads to the effective chemiluminescence. The successful quantitative assay of H_2O_2 by the Cu^{2+}-NMOFs was then applied to develop a glucose sensor. The aerobic oxidation of glucose, in the presence of glucose oxidase, GOx, yields gluconic acid and H_2O_2. As the concentration of H_2O_2 relates to the concentration of glucose, the sequestered detection of the biocatalytically generated H_2O_2 by the Cu^{2+}-NMOFs stimulated generation of chemiluminescence, in the presence of luminol, provides a readout signal for the quantitative detection of glucose. Figure 4D shows the chemiluminescence spectra generated in the presence of different concentrations of glucose. Figure 4D (inset) shows the resulting calibration curve.

As stated, recent studies reported on diverse nanoparticles that mimic peroxidase functions. It should be noted, however, that a fair comparison between the catalytic peroxidase-mimicking activities of the different nanoparticles is difficult due to the following reasons: (i) the different nanoparticles do not mimic all peroxidase functions, while some of them mimic several peroxidase functions other peroxidase functions are lacking. (ii) Quantitative information addressing the concentrations of the catalytic sites in the bulk weight supports is missing. To address the catalytic functions of the Cu^{2+}-NMOFs

Table 1. Comparison of the catalytic performance of different Cu^{2+}-ion-functionalized nanoparticles toward the catalyzed oxidation of dopamine to aminochrome by H_2O_2.

System	V_{max} [mg NPs mL^{-1} solution]	Content of Cu^{2+} ions [wt%]	Ref.
Cu^{2+}-graphene oxide NPs	0.3	21	[25]
Cu^{2+}-C_3N_4 NPs	0.24	4.6	[24]
Cu^{2+}-C-dots	0.7	14	[24]
Cu^{2+}-$Fe^{2+/3+}$-cyanometalates	0.34	17.8	[33]
Cu^{2+}-NMOFs	0.095	5.5	This study

as compared to other Cu^{2+}-ion-functionalized nanocatalysts, we selected several Cu^{2+}-ion catalytic systems that identified the content of the catalytic sites, and compared the systems toward the identical peroxidase-mimicking transformation, e.g., the catalyzed oxidation of dopamine to aminochrome. The results are summarized in **Table 1**. One may realize that the Cu^{2+}-NMOFs exhibit lower catalytic performance toward the oxidation of dopamine to aminochrome by H_2O_2. For example, the Cu^{2+} ions loading on the Cu^{2+}-C_3N_4 is very similar to the Cu^{2+} loading on the Cu^{2+}-NMOFs. The catalytic activity of the latter catalyst is, however, ≈2-fold lower. Similarly, the Cu^{2+} loading of the Cu^{2+}-C-dots is ≈3-fold higher as compared to the Cu^{2+} content in the Cu^{2+}-NMOFs, and the catalytic performance of the Cu^{2+}-C-dots is ≈2.3-fold higher as compared to the Cu^{2+}-NMOFs. The advantages of the Cu^{2+}-NMOFs are reflected, however, by the many chemical transformations that mimic native peroxidases by these catalytic nanoparticles, vide infra.

The Cu^{2+}-NMOFs, also, mimic the functions of NADH-peroxidase. In this system, the Cu^{2+}-NMOFs-catalyzed oxidation of NADH to NAD^+ by H_2O_2 proceeds (**Figure 5**A). Figure 5B shows the time-dependent oxidation of different concentrations of NADH (probed by following the decrease in the absorbance of NADH at λ = 340 nm) in the presence of H_2O_2, 2×10^{-3} M and Cu^{2+}-NMOFs, 20 μg mL^{-1}. As the concentration of NADH increases, the rate of oxidation of NADH is enhanced (Figure 5B, inset). The rate of NADH oxidation is, also, controlled by the concentration of the Cu^{2+}-NMOFs (see Figure S8, Supporting Information) and by the concentration of H_2O_2. Figure 5C shows the rate of oxidation of NADH by different concentrations of H_2O_2 (fixed concentrations of NADH, 0.5×10^{-3} M, and of Cu^{2+}-NMOFs, 20 μg mL^{-1}). For the resulting calibration curve showing the rate of NADH oxidation as a function of H_2O_2 concentration, see Figure S9 (Supporting Information). An important issue that needs to be addressed relates to the proof that NADH is oxidized to the biologically active cofactor, NAD^+, rather than to the biologically inactive cofactor dimer $(NAD)_2$. To

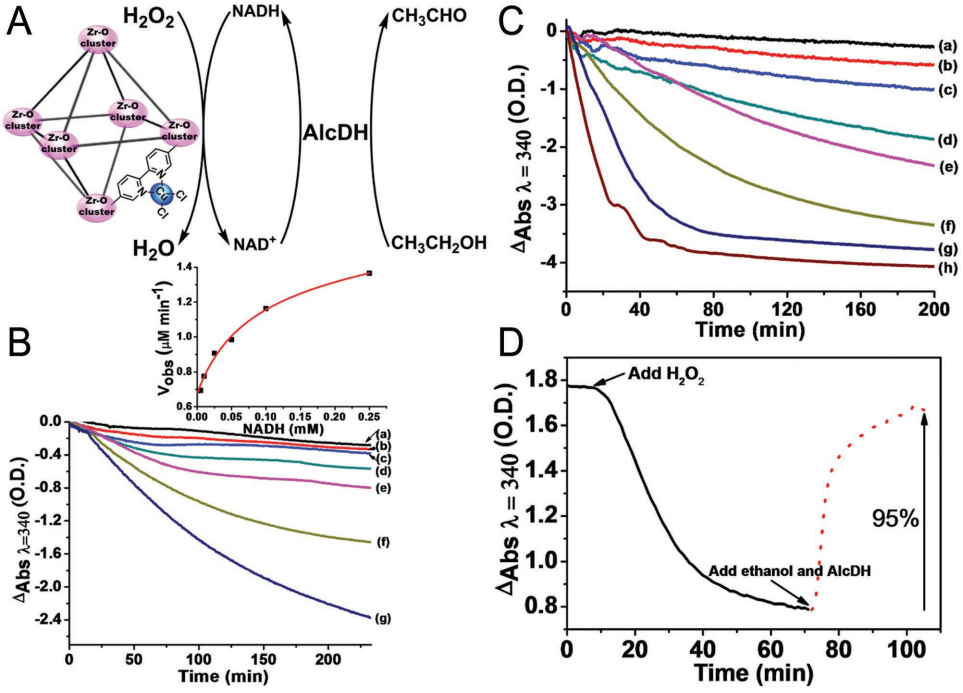

Figure 5. A) Schematic Cu^{2+}-NMOFs-catalyzed oxidation of NADH to NAD^+ by H_2O_2 and the application of the catalytic process as a NAD^+-regeneration process for biocatalytic transformations. B) Time-dependent absorbance changes upon the Cu^{2+}-NMOFs (20 μg mL^{-1}) catalyzed oxidation of different concentrations of NADH by H_2O_2 2×10^{-3} M. NADH concentrations correspond to: (a) 0 M, (b) 0.005×10^{-3} M, (c) 0.01×10^{-3} M, (d) 0.025×10^{-3} M, (e) 0.05×10^{-3} M, (f) 0.1×10^{-3} M, (g) 0.25×10^{-3} M. Inset: calibration curve corresponding to the rate of NADH oxidation as a function of NADH concentration. C) Time-dependent absorbance changes upon the Cu^{2+}-NMOFs-catalyzed oxidation of NADH, 0.5×10^{-3} M, by different concentrations of H_2O_2: (a) 0 M, (b) 0.1×10^{-3} M, (c) 0.2×10^{-3} M, (d) 0.5×10^{-3} M, (e) 1×10^{-3} M, (f) 2×10^{-3} M, (g) 5×10^{-3} M, (h) 10×10^{-3} M. D) Time-dependent absorbance changes upon the Cu^{2+}-NMOFs-catalyzed oxidation of NADH by H_2O_2 to form NAD^+ and the subsequent regeneration of NADH by the AlcDH-catalyzed oxidation of ethanol to acetaldehyde. The initial solid curve represents the time-dependent Cu^{2+}-NMOFs-catalyzed oxidation of NADH by H_2O_2 (Cu^{2+}-NMOFs 20 μg mL^{-1}, NADH 0.1×10^{-3} M, and H_2O_2 2×10^{-3} M). At the point marked with an arrow ethanol 30×10^{-3} M and AlcDH 50 U were added to the system, resulting in the recovery of NADH.

confirm the formation of the NAD^+ cofactor, the Cu^{2+}-NMOFs-catalyzed oxidation of NADH by H_2O_2 was activated for 60 min to allow the depletion of the NADH absorbance, Figure 5D. Afterward, ethanol and the enzyme alcohol dehydrogenase, AlcDH, were added to the system. The spectral features of NADH were recovered by ≈95% and the absorbance of the recovered NADH retained a steady-state value. The recovery of the NADH absorbance implies that the biologically active NAD^+ cofactor was formed as a result of the NAD^+-dependent AlcDH-catalyzed oxidation of ethanol to acetaldehyde. Furthermore, we note that after completion of the oxidation of NADH to NAD^+ by the H_2O_2, the Cu^{2+}-NMOFs were precipitated, and the separated Cu^{2+}-NMOFs were reapplied for the catalyzed oxidation of NADH. The Cu^{2+}-NMOFs catalytic function was unaffected and the oxidation of NADH followed the results shown in Figure 5. These experiments were repeated three times and only a minute effect on the activities of the Cu^{2+}-NMOFs was observed (≈10% decrease in the activity due to the loss of the Cu^{2+}-NMOFs in the separation steps). These results imply that the Cu^{2+}-NMOFs provide an effective catalyst for the oxidation of NADH to NAD^+. Note that control experiments revealed that Cu^{2+} ions or Cu^{2+} ions in the presence of the bipyridine ligand (at similar molar concentrations existing in the NMOFs) did not show any NADH peroxidase activities under identical conditions used with the Cu^{2+}-NMOFs, thus demonstrating the unique catalytic properties of Cu^{2+}-NMOFs as NADH peroxidase-mimicking nanoenzymes. The effective Cu^{2+}-NMOFs-catalyzed oxidation of NADH by H_2O_2 is attributed to the concentration of NADH in the porous structure of the NMOFs, in close proximity to the catalytic sites. This is supported by complementary surface area analysis. While the Cu^{2+}-NMOFs revealed a surface area of 246 $m^2\ g^{-1}$ and average pore size of 1.65 nm, the NMOFs treated with NADH exhibited a surface area corresponding to 142 $m^2\ g^{-1}$ and pore size of 1.26 nm, respectively. The lower surface area and decrease in the pore size of the NMOFs, after their treatment with NADH, imply that the pores are loaded with the NADH substrate. Beyond the demonstration that the Cu^{2+}-NMOFs act as an NADH-peroxidase-mimicking catalyst, the system introduces a novel mean to regenerate the NAD^+ cofactor, thus allowing the application of the NMOFs as catalyst to drive biotechnological processes driven by NAD^+-dependent enzymes.

Finally, we applied the Cu^{2+}-NMOFs as a functional material for stimulating a CRET process. Previous studies indicated that the chemiluminescence generated by HRP using the luminol/H_2O_2 system can induce, albeit at very low efficiency, a CRET process to organic dyes, e.g., fluorescein.[29] Also, the hemin/G-quadruplex HRP-mimicking DNAzyme linked to semiconductor quantum dots[30] or associated in supramolecular complexes with organic dyes[31] leads, in the presence of luminol/H_2O_2, to inefficient CRET processes that result in the luminescence of the quantum dots or the fluorescence of the organic dyes, without external excitation of the chromophores. The porous structure of the Cu^{2+}-NMOFs suggested that the incorporation of an acceptor dye in the porous material in close proximity to the catalytic chemiluminescence Cu^{2+}-NMOFs sites could stimulate the CRET process. Accordingly, the Cu^{2+}-NMOFs were loaded with the fluorescein dye (**Figure 6**A). The

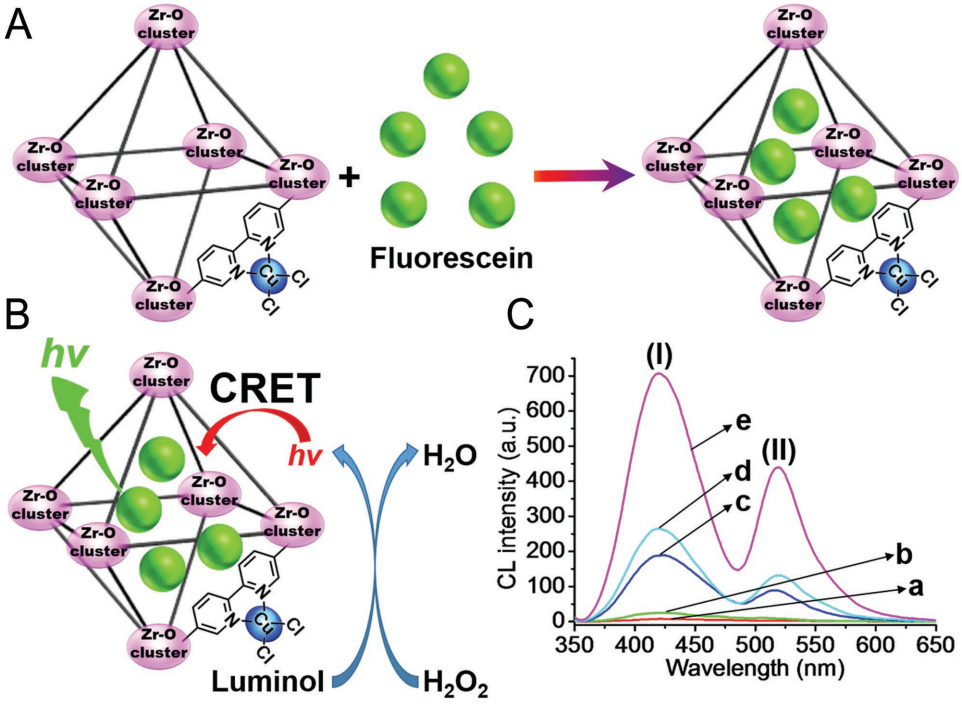

Figure 6. A) Incorporation of fluorescein to Cu^{2+}-NMOFs. B) The stimulation of the chemiluminescence resonance energy transfer (CRET) from the Cu^{2+}-NMOFs to fluorescein in the presence of luminol/H_2O_2. The CRET process leads to the fluorescence of fluorescein at $\lambda = 520$ nm. C) Luminescence spectra comprising the luminol/H_2O_2 chemiluminescence band (I) and the fluorescence band of fluorescein generated by the CRET process (II) in the presence of different concentrations of the NMOFs: (a) 10 μg mL^{-1}, (b) 20 μg mL^{-1}, (c) 50 μg mL^{-1}, (d) 75 μg mL^{-1}, (e) 100 μg mL^{-1}. In all experiments luminol 0.5×10^{-3} M and H_2O_2 5×10^{-3} M were used.

dye-loaded Cu^{2+}-NMOFs were subjected to the luminol/H_2O_2 chemiluminescence generation system (Figure 6B). Figure 6C depicts the luminescence spectrum of the system. Interestingly, besides the chemiluminescence spectrum of the luminol/H_2O_2 system, at 425 nm, an intense fluorescence band of fluorescein at $\lambda = 520$ nm is observed. The fluorescence of fluorescein is originated from a CRET process in the Cu^{2+}-NMOFs. Control experiments revealed that no CRET-induced fluorescence of fluorescein is observed in the presence of Cu^{2+} ions or Cu^{2+}/bipyridine ligand assemblies. From the intensity of the absorbance band of fluorescein, we estimated[32] the CRET efficiency to be 35%. This unprecedented CRET efficiency is attributed to the concentration of the acceptor dye in the porous matrix of the NMOFs in close spatial proximity to the dense catalytic sites of Cu^{2+}-NMOFs. These CRET generating NMOFs could be applied as optical reporter for sensors, e.g., metal ions (Cu^{2+}) or biosensors, e.g., probing H_2O_2 generated by oxidases.

In conclusion, the present study has introduced Cu^{2+}-modified bipyridine-functionalized UiO-type NMOFs as catalytic nanoparticles (nanoenzymes) that mimic peroxidase functions. Specifically, we demonstrated that the Cu^{2+}-NMOFs mimic HRP by oxidizing Amplex-Red by H_2O_2 to form Resorufin, by oxidizing dopamine to aminochrome by H_2O_2, and by catalyzing the generation of chemiluminescence in the presence of luminol/H_2O_2. Also, the Cu^{2+}-NMOFs acted as NADH peroxidase-mimicking catalysts, i.e, the nanoparticles catalyzed the oxidation of NADH to NAD^+ by H_2O_2. Beyond the ability to mimic enzyme functions by the NMOFs (nanoenzymes), the system can be used to develop different sensors, e.g., for glucose or NADH, and as a NAD^+-regeneration system to drive biocatalytic synthetic transformations that apply NAD^+-dependent enzyme. The unprecedented efficient CRET process that proceeds between the Cu^{2+}-NMOFs catalytic sites and the dye entrapped in the porous NMOFs paves the way to design novel NMOFs sensing platforms. Furthermore, the successful assembly of the Cu^{2+}-modified bipyridine-based UiO-type NMOFs as catalysts suggests that other metal ions, such as Rh^{3+}, Zn^{2+}, or Ru^{2+}, could be linked to the NMOFs to yield catalytic and photocatalytic systems for other chemical transformations.

Experimental Section

Detailed synthesis and characterizations are reported in the Supporting Information.

Supporting Information

Supporting Information is available from the Wiley Online Library or from the author.

Acknowledgements

This research was supported by the MINERVA Center for Bio-hybrid Complex Systems.

Conflict of Interest

The authors declare no conflict of interest.

Keywords

chemiluminescence resonance energy transfer (CRET), dopamine, glucose, NADH, sensors

Received: September 18, 2017
Revised: October 15, 2017
Published online:

[1] a) H. Furukawa, K. E. Cordova, M. O'Keeffe, O. M. Yaghi, *Science* **2013**, *341*, 1230444; b) M. P. Suh, H. J. Park, T. K. Prasad, D. W. Lim, *Chem. Rev.* **2012**, *112*, 782; c) Y. Cui, B. Li, H. He, W. Zhou, B. Chen, G. Qian, *Acc. Chem. Res.* **2016**, *49*, 483.
[2] H. C. Zhou, S. Kitagawa, *Chem. Soc. Rev.* **2014**, *43*, 5415.
[3] a) N. Li, J. Xu, R. Feng, T. L. Hu, X. H. Bu, *Chem. Commun.* **2016**, *52*, 8501; b) Z. Chang, D. H. Yang, J. Xu, T. L. Hu, X. H. Bu, *Adv. Mater.* **2015**, *27*, 5432; c) Q. Gao, J. Xu, D. Cao, Z. Chang, X. H. Bu, *Angew. Chem., Int. Ed.* **2016**, *55*, 15027.
[4] a) C. He, K. Lu, D. Liu, W. Lin, *J. Am. Chem. Soc.* **2014**, *136*, 5181; b) P. Horcajada, R. Gref, T. Baati, P. K. Allan, G. Maurin, P. Couvreur, G. Férey, R. E. Morris, C. Serre, *Chem. Rev.* **2012**, *112*, 1232; c) P. Horcajada, T. Chalati, C. Serre, B. Gillet, C. Sebrie, T. Baati, J. F. Eubank, D. Heurtaux, P. Clayette, C. Kreuz, J. S. Chang, Y. K. Hwang, V. Marsaud, P. N. Bories, L. Cynober, S. Gil, G. Férey, P. Couvreur, R. Gref, *Nat. Mater.* **2010**, *9*, 172.
[5] a) L. Ma, W. Lin, *Top. Curr. Chem.* **2010**, *293*, 175; b) A. Dhakshinamoorthy, H. Garcia, *Chem. Soc. Rev.* **2012**, *41*, 5262; c) A. Corma, H. García, F. X. Llabrés i Xamena, *Chem. Rev.* **2010**, *110*, 4606; d) F. Song, C. Wang, J. M. Falkowski, L. Ma, W. Lin, *J. Am. Chem. Soc.* **2010**, *132*, 15390; e) C. Zhu, G. Yuan, X. Chen, Z. Yang, Y. Cui, *J. Am. Chem. Soc.* **2012**, *134*, 8058.
[6] a) M. J. Dong, M. Zhao, S. Ou, C. Zou, C. D. Wu, *Angew. Chem., Int. Ed.* **2014**, *53*, 1575; b) I. H. Park, R. Medishetty, J. Y. Kim, S. S. Lee, J. J. Vittal, *Angew. Chem., Int. Ed.* **2014**, *53*, 5591; c) J. Ferrando-Soria, H. Khajavi, P. Serra-Crespo, J. Gascon, F. Kapteijn, M. Julve, F. Lloret, J. Pasán, C. Ruiz-Pérez, Y. Journaux, E. Pardo, *Adv. Mater.* **2012**, *24*, 5625; d) Y. Lu, B. Yan, J. L. Liu, *Chem. Commun.* **2014**, *50*, 9969.
[7] a) M. P. Suh, H. J. Park, T. K. Prasad, D. W. Lim, *Chem. Rev.* **2012**, *112*, 782; b) Y. Yan, S. Yang, A. J. Blake, M. Schröder, *Acc. Chem. Res.* **2014**, *47*, 296; c) H. W. Langmi, J. Ren, B. North, M. Mathe, D. Bessarabov, *Electrochim. Acta* **2014**, *128*, 368.
[8] a) J. R. Li, J. Sculley, H. C. Zhou, *Chem. Rev.* **2012**, *112*, 869; b) N. A. Khan, Z. Hasan, S. H. Jhung, *J. Hazard. Mater.* **2013**, *244*, 444.
[9] a) C. D. Müller, A. Falcou, N. Reckefuss, M. Rojahn, V. Wiederhirn, P. Rudati, H. Frohne, O. Nuyken, H. Becker, K. Meerholz, *Nature* **2003**, *421*, 829; b) V. Stavila, A. A. Talin, M. D. Allendorf, *Chem. Soc. Rev.* **2014**, *43*, 5994; c) T. C. Chao, Y. T. Lin, C. Y. Yang, T. S. Hung, H. C. Chou, C. C. Wu, K. T. Wong, *Adv. Mater.* **2005**, *17*, 992.
[10] D. Kim, D. R. Whang, S. Y. Park, *J. Am. Chem. Soc.* **2016**, *138*, 8698.
[11] J. Li, X. Yu, M. Xu, W. Liu, E. Sandraz, H. Lan, J. Wang, S. M. Cohen, *J. Am. Chem. Soc.* **2017**, *139*, 611.
[12] a) J. Lee, O. K. Farha, J. Roberts, K. A. Scheidt, S. T. Nguyen, J. T. Hupp, *Chem. Soc. Rev.* **2009**, *38*, 1450; b) J. Liu, L. Chen, H. Cui, J. Zhang, L. Zhang, C. Y. Su, *Chem. Soc. Rev.* **2014**, *43*, 6011; c) A. Corma, H. García, F. X. Llabrés i Xamena, *Chem. Rev.* **2010**, *110*, 4606.
[13] F. Luo, Y. Lin, L. Zheng, X. Lin, Y. Chi, *ACS Appl. Mater. Interfaces* **2015**, *7*, 11322.
[14] K. Manna, T. Zhang, W. Lin, *J. Am. Chem. Soc.* **2014**, *136*, 6566.
[15] A. G. Roth, D. Drescher, Y. Yang, S. Redmer, S. Uhlig, C. Arenz, *Angew. Chem., Int. Ed.* **2009**, *48*, 7560.

[16] a) K. Tabatabaeian, M. Ali Zanjanchi, O. Mahmoodi, T. Eftekhari, *Lett. Org. Chem.* **2017**, *14*, 207; b) S. Mandal, P. C. Rao, *ChemCatChem* **2017**, *9*, 1172.
[17] a) B. An, J. Zhang, K. Cheng, P. Ji, C. Wang, W. Lin, *J. Am. Chem. Soc.* **2017**, *139*, 3834; b) B. Tang, W. C. Song, E. C. Yang, X. J. Zhao, *RSC Adv.* **2017**, *7*, 1531; c) Q. Yang, Q. Xu, S. H. Yu, H. L. Jiang, *Angew. Chem., Int. Ed.* **2016**, *55*, 3685.
[18] a) K. Tabatabaeian, M. A. Zanjanchi, N. O. Mahmoodi, T. Eftekhari, *RSC Adv.* **2015**, *5*, 101013; b) C. Bai, A. Li, X. Yao, H. Liu, Y. Li, *Green Chem.* **2016**, *18*, 1061.
[19] a) P. Travascio, Y. Li, D. Sen, *Chem. Biol.* **1998**, *5*, 505; b) P. Travascio, A. J. Bennet, D. Y. Wang, D. Sen, *Chem. Biol.* **1999**, *6*, 779.
[20] a) M. Comotti, C. Della Pina, R. Matarrese, M. Rossi, *Angew. Chem., Int. Ed.* **2004**, *43*, 5812; b) Y. Zhao, Y. Huang, H. Zhu, Q. Zhu, Y. Xia, *J. Am. Chem. Soc.* **2016**, *138*, 16645.
[21] M. B. Gawande, A. Goswami, F. X. Felpin, T. Asefa, X. Huang, R. Silva, X. Zou, R. Zboril, R. S. Varma, *Chem. Rev.* **2016**, *116*, 3722.
[22] E. Golub, G. Pelossof, R. Freeman, H. Zhang, I. Willner, *Anal. Chem.* **2009**, *81*, 9291.
[23] a) J. Chen, S. Patil, S. Seal, J. F. McGinnis, *Nat. Nanotechnol.* **2006**, *1*, 142; b) F. Natalio, R. André, A. F. Hartog, B. Stoll, K. P. Jochum, R. Wever, W. Tremel, *Nat. Nanotechnol.* **2012**, *7*, 530.
[24] M. Vázquez-González, W. C. Liao, R. Cazelles, S. Wang, X. Yu, V. Gutkin, I. Willner, *ACS Nano* **2017**, *11*, 3247.
[25] S. Wang, R. Cazelles, W. C. Liao, M. Vázquez-González, A. Zoabi, R. Abu-Reziq, I. Willner, *Nano Lett.* **2017**, *17*, 2043.
[26] a) X. Yi, W. Dong, X. Zhang, J. Xie, Y. Huang, *Anal. Bioanal. Chem.* **2016**, *408*, 8805; b) N. Yang, H. Song, X. Wan, X. Fan, Y. Su, Y. Lv, *Analyst* **2015**, *140*, 2656.
[27] S. Wang, W. Morris, Y. Liu, C. M. McGuirk, Y. Zhou, J. T. Hupp, O. K. Farha, C. A. Mirkin, *Angew. Chem., Int. Ed.* **2015**, *54*, 14738.
[28] a) Y. Hu, H. Cheng, X. Zhao, J. Wu, F. Muhammad, S. Lin, J. He, L. Zhou, C. Zhang, Y. Deng, P. Wang, Z. Zhou, S. Nie, H. Wei, *ACS Nano* **2017**, *11*, 5558; b) H. Liang, F. Lin, Z. Zhang, B. Liu, S. Jiang, Q. Yuan, J. Liu, *ACS Appl. Mater. Interfaces* **2017**, *9*, 1352; c) X. Yi, W. Dong, X. Zhang, J. Xie, Y. Huang, *Anal. Bioanal. Chem.* **2016**, *408*, 8805.
[29] A. Navas Díaz, J. A. González García, J. Lovillo, *J. Biolumin. Chemilumin.* **1997**, *12*, 199.
[30] R. Freeman, X. Liu, I. Willner, *J. Am. Chem. Soc.* **2011**, *133*, 11597.
[31] X. Liu, A. Niazov-Elkan, F. Wang, I. Willner, *Nano Lett.* **2013**, *13*, 219.
[32] Z. Li, Y. Wang, G. Zhang, W. Xu, Y. Han. *J. Lumin.* **2010**, *130*, 995.
[33] M. Vázquez-González, R. M. Torrente-Rodríguez, A. Kozell, W. C. Liao, A. Cecconello, S. Campuzano, J. M. Pingarrón, I. Willner, *Nano Lett.* **2017**, *17*, 4958.